Analysis of Algorithms Generalizing B-Spline Subdivision

Jörg Peters* Ulrich Reif†

January 27, 1997

Abstract

A new set of tools for verifying smoothness of surfaces generated by stationary subdivision algorithms is presented. The main challenge here is the verification of injectivity of the characteristic map. The tools are sufficiently versatile and easy to wield to allow, as an application, a full analysis of algorithms generalizing biquadratic and bicubic B-spline subdivision. In the case of generalized biquadratic subdivision the analysis yields a hitherto unknown sharp bound strictly less than one on the second largest eigenvalue of any smoothly converging subdivision.

Keywords: subdivision, arbitrary topology, characteristic map, Doo-Sabin Algorithm, Catmull-Clark algorithm, B-spline
AMS subject classification: 65D17, 65D07, 68U07
Abbreviated title: Generalized B-Spline Subdivision

1 Introduction

The idea of generating smooth free-form surfaces of arbitrary topology by iterated mesh refinement dates back to 1978, when two papers [CC78], [DS78] appeared back to back in the same issue of Computer Aided Design. Named after their inventors, the Doo-Sabin and the Catmull-Clark algorithm represent generalizations of the subdivision schemes for biquadratic and bicubic B-splines, respectively. By combining a construction principle of striking simplicity with high fairness of the generated surfaces, both algorithms have since become standard tools in Computer Aided Geometric Design. However, despite a number of attempts [DS78], [BS86], [BS88], the convergence to smooth limit surfaces could not be proven rigorously so far.

*NSF National Young Investigator Award 9457806-CCR
†BMBF Projekt 03–HO7STU–2

The proof techniques and actual proofs to be presented here are based on the concept of the *characteristic map* as introduced in [Rei95a]. The characteristic map is a smooth map from some compact domain U to $\mathbb{R}^2$ which can be assigned to stationary linear subdivision schemes. It depends only on the structure of the algorithm and not on the data. If this map is both regular and injective, then the corresponding algorithm generates C^1-limit surfaces. It is shown in this paper that on the other hand non-injectivity at an interior point of the map implies non-smoothness of the limit surfaces. Further, we establish two sufficient conditions for regularity and injectivity of the characteristic map which allow a straightforward verification. The stronger one, however still applicable in many cases, only requires the sign of one partial derivative of one segment of the characteristic map to be positive.

A careful analysis of the Doo-Sabin and the Catmull Clark algorithm yields the following results:

- The Doo-Sabin algorithm in its general form uses weights $\alpha = (\alpha^0, \ldots, \alpha^{n-1})$ for computing a new n-gon from an old one. Affine invariance and symmetry, i.e. $\sum_j \alpha^j = 1$ and $\alpha^j = \alpha^{n-j}$ for all $j \mod n$, imply that the discrete Fourier transform of α is real and of the form $\hat{\alpha} = [1, \hat{\alpha}^1, \hat{\alpha}^2, \ldots, \hat{\alpha}^2, \hat{\alpha}^1]$. If $\lambda := \hat{\alpha}^1$ is greater in modulus than the other entries except for 1 and if

$$1/4 < \lambda < \lambda_{\max}(n) \tag{1.1}$$

  for certain values $\lambda_{\max}(n) < 1$ then the limit surface is smooth. The bound $\lambda_{\max}(n)$ can be computed explicitly, see Table 1. If $1 > \lambda > \lambda_{\max}(n)$, then the limit is a continuous, yet non-smooth surface.

- In particular, the Doo-Sabin algorithm in its original form (5.1) complies with the conditions, hence generates smooth limit surfaces.

- The Catmull-Clark algorithm in its general form uses three weights α, β, γ summing up to one for computing the new location of an extraordinary vertex from its predecessor and the centers of its neighbors. If

$$2 \left| 4\alpha - 1 \pm \sqrt{(4\alpha - 1)^2 + 8\beta - 4} \right| < c_n + 5 + \sqrt{(c_n + 9)(c_n + 1)} \tag{1.2}$$

  with $c_n := \cos(2\pi/n)$, then the limit surface is smooth. If one of the two values on the left hand side exceeds the right hand side, then the limit surface is not smooth.

- In particular, the Catmull-Clark algorithm in its original form (6.2) complies with the conditions and generates smooth limit surfaces.

2 Generalized subdivision and the characteristic map

In this section we briefly outline the results of subdivision analysis as developed in [Rei95a], and establish a new necessary condition for C^1-subdivision schemes.

Generalized B-spline subdivision generates a sequence $\mathbf{C}_m$ of finer and finer control polyhedra converging to some limit surface $\mathbf{y}$. On the regular part of the mesh, standard B-spline subdivision is used for refinement, whereas special rules apply near extraordinary mesh points. Since all subdivision masks considered here are of fixed finite size, we can restrict ourselves to analyzing meshes with a single extraordinary mesh point of valence $n \neq 4$. The regular parts of the control polygons $\mathbf{C}_m$ correspond to B-spline surfaces $\mathbf{y}_m$ which form an ascending sequence

$$\mathbf{y}_0 \subset \mathbf{y}_1 \subset \mathbf{y}_2 \subset \cdots \tag{2.1}$$

converging to the limit surface,

$$\mathbf{y} = \bigcup_{m \in \mathbb{N}} \mathbf{y}_m \ . \tag{2.2}$$

With the prolongation of $\mathbf{y}_m$ defined by

$$\mathbf{x}_m := \text{closure}\,(\mathbf{y}_{m+1} \backslash \mathbf{y}_m) \ , \tag{2.3}$$

the limit surface is the essentially disjoint[1] union

$$\mathbf{y} = \mathbf{y}_0 \cup \bigcup_{m \in \mathbb{N}} \mathbf{x}_m \ . \tag{2.4}$$

The $\mathbf{x}_m$ are ring-shaped *surface layers* which can be parametrized conveniently over a common domain $U \times \mathbb{Z}_n, \mathbb{Z}_n := \mathbb{Z} \mod n$, consisting of n copies of the compact set

$$U := [0,2]^2 \backslash [0,1)^2 \ , \tag{2.5}$$

see Figure 1. Each surface layer $\mathbf{x}_m$ can be parametrized in terms of control points $\mathbf{B}_m^k \in \mathbb{R}^3$ and piecewise polynomial functions N^ℓ according to

$$\mathbf{x}_m : U \times \mathbb{Z}_n \ni (u,v,j) \mapsto \mathbf{x}_m^j(u,v) = \sum_{\ell=0}^{L} N^\ell(u,v,j) \mathbf{B}_m^\ell \ . \tag{2.6}$$

Without loss of generality, we may assume that the functions N^ℓ are linearly independent. Otherwise, the setup can be reduced without altering the properties of the scheme. The n parts $\mathbf{x}_m^0, \ldots, \mathbf{x}_m^{n-1}$ forming $\mathbf{x}_m$ are referred to as *segments*. Collecting

[1] The intersection consists exclusively of points on the common boundary curve, which are identified.

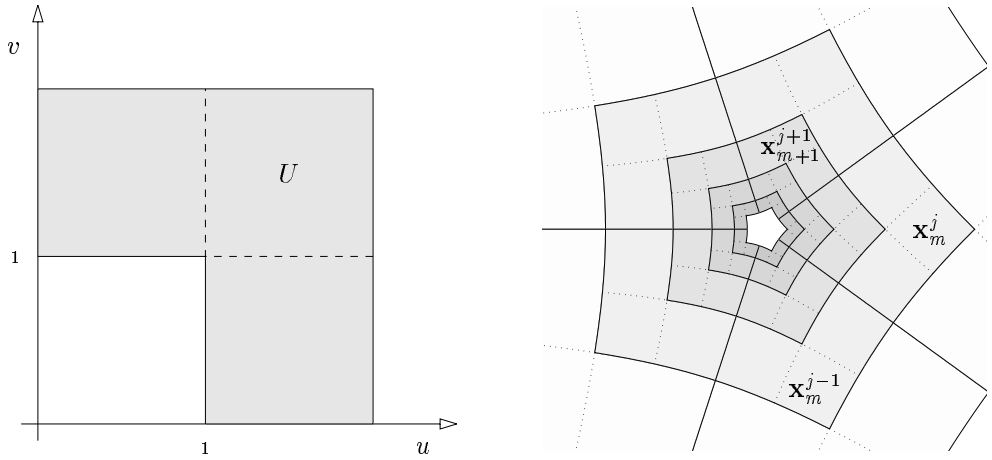

Figure 1: Domain U *(left)* and structure of surface layers $\mathbf{x}_m$ *(right)*.

the functions N^ℓ in the columns of a row matrix N and the control points in the rows of a column matrix $\mathbf{B}_m$ yields the vector notation

$$\mathbf{x}_m(u,v,j) = \mathbf{x}_m^j(u,v) = N(u,v,j)\mathbf{B}_m \ . \tag{2.7}$$

The schemes to be considered here are *linear* and *stationary*, i.e. there exists a square *subdivision matrix* A with

$$\mathbf{B}_{m+1} = A\mathbf{B}_m \ . \tag{2.8}$$

Definition 2.1 *Let the eigenvalues* $\lambda_0, \ldots, \lambda_L$ *of* A *be ordered by modulus,*

$$|\lambda_0| \geq |\lambda_1| \geq \cdots \geq |\lambda_L| \ , \tag{2.9}$$

and denote by $\psi_0, \ldots, \psi_L$ *the corresponding generalized real eigenvectors. If* $|\lambda_0| > |\lambda_1| = |\lambda_2| > |\lambda_3|$ *then the* characteristic map *of the subdivision algorithm is defined by*

$$\Psi := N[\psi_1, \psi_2] \ : \ U \times \mathbb{Z}_n \to \mathbb{R}^2 \ , \tag{2.10}$$

or in complex form by

$$\Psi_* := N\psi_* \ : \ U \times \mathbb{Z}_n \to \mathbb{C} \ , \quad \psi_* := \psi_1 + i\psi_2 \ . \tag{2.11}$$

Following (2.7)*, the* segments Ψ^j *and* Ψ_*^j *of the characteristic map are the restriction of* Ψ *and* Ψ_* *to* $U \times j$*, respectively.*

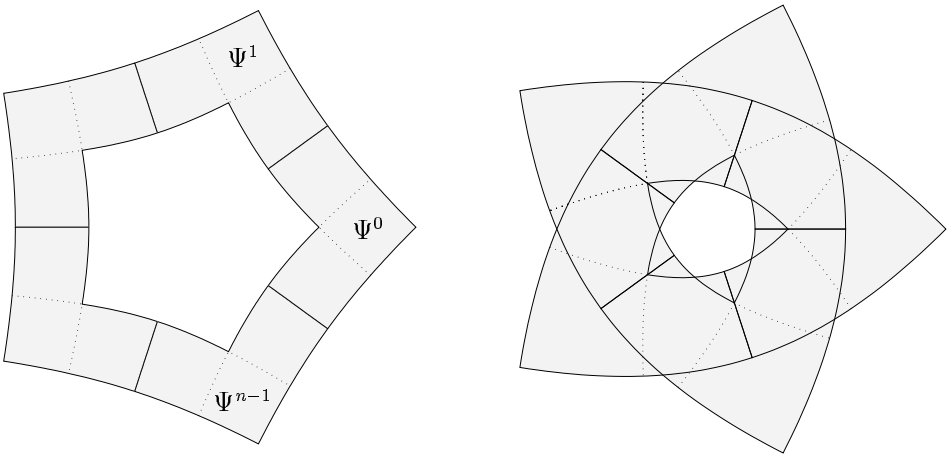

Figure 2: Injective *(left)* and non-injective *(right)* characteristic map

Remark *i)* $[\psi_1, \psi_2]$ is a $(L+1) \times 2$-matrix. Its rows play the role of 2D control points. *ii)* Throughout, the subscript $*$ will indicate that we refer to the complexification of a two-dimensional real variable or function. We will switch between complex and real representation without further notice.

On the left hand side, Figure 2 shows a typical example of a characteristic map for $n = 5$ as obtained for example by the Doo-Sabin algorithm. In order to guarantee affine invariance of the algorithm, the rows of A must sum to 1. Thus, $(1, \ldots, 1)$ is always an eigenvector of A to the eigenvalue 1. The following theorem establishes a sufficient condition for subdivision algorithms to generate smooth limit surfaces.

Theorem 2.1 *If $\lambda := \lambda_1 = \lambda_2$, $1 > \lambda > |\lambda_3|$, is a real eigenvalue with geometric multiplicity 2, and if the characteristic map is regular and injective, then the limit surface $\mathbf{y}$ is a regular C^1-manifold for almost every choice of initial data $\mathbf{B}_0$.*

A proof of this theorem can be found in [Rei95a]. Generalizations, though not required here, are provided in [Rei95b] and [PR97]. Subsequently, it will be assumed that the eigenvalues of A satisfy the assumptions of Theorem 2.1, and λ will be referred to as the *subdominant eigenvalue*.

The following theorem states a necessary condition for the convergence of a subdivision scheme to smooth limit surfaces.

Theorem 2.2 *If the characteristic map of a subdivision scheme is non-injective, i.e. there exist $(u, v, j) \neq (u', v', j')$ such that*

$$\Psi(u, v, j) = \Psi(u', v', j') \ , \tag{2.12}$$

and if $\Psi(u,v,j)$ is an interior point of $\Psi(U,\mathbb{Z}_n)$, then the limit surface $\mathbf{y}$ *is not a regular C^1-manifold for almost every choice of initial data* $\mathbf{B}_0$.

Proof Choose an ε-neighborhood $V_\varepsilon(\Psi(u,v,j))$ such that $V_\varepsilon(\Psi(u,v,j)) \subset \Psi(U,\mathbb{Z}_n)$. Then there exist neighborhoods V and V' of (u,v,j) and (u',v',j'), respectively, with $\Psi(V) = \Psi(V') = V_\varepsilon(\Psi(u,v,j))$. If $\tilde{\Psi}$ is a continuous map sufficiently close to Ψ, i.e. $\|\Psi - \tilde{\Psi}\|_\infty < \varepsilon/2$, then $\tilde{\Psi}(V) \cap \tilde{\Psi}(V') \neq \emptyset$ and $\tilde{\Psi}$ is also not injective. Now, express $\mathbf{B}_m$ in terms of the generalized eigenvectors ψ_ℓ,

$$\mathbf{B}_0 = \sum_{\ell=0}^{L} \psi_\ell \mathbf{b}_\ell \ , \quad \mathbf{B}_m = \mathbf{b}_0 + \lambda^m(\psi_1 \mathbf{b}_1 + \psi_2 \mathbf{b}_2) + o(|\lambda|^m) \ . \tag{2.13}$$

Then for almost every choice of initial data $\mathbf{B}_0$, the coefficients $\mathbf{b}_1$ and $\mathbf{b}_2$ are linearly independent, and we can choose coordinates such that $\mathbf{b}_0 = \mathbf{0}$ is the origin and $\mathbf{b}_1 = \mathbf{e}_1, \mathbf{b}_2 = \mathbf{e}_2$ are the first two unit vectors. A rescaling of the surface layers yields

$$\tilde{\mathbf{x}}_m := \lambda^{-m}\mathbf{x}_m = \mathbf{e}_1\psi_1 + \mathbf{e}_2\psi_2 + o(1) = (\Psi, 0) + o(1) \quad \text{as} \quad m \to \infty \ . \tag{2.14}$$

Now, assume that $\mathbf{y}$ is a regular C^1-manifold. Then the latter equation implies that the tangent plane at the origin is the xy-plane. The projection $\tilde{\psi}_m$ of $\tilde{\mathbf{x}}_m$ on the xy-plane is converging to Ψ, so $\tilde{\psi}_m$ is non-injective for m sufficiently large. Consequently, the projection of the layers $\mathbf{x}_m$ to the xy-plane are non-injective near the origin for almost all m. This contradicts the assumption since the projection of a regular C^1-manifold on its tangent plane is locally injective. □

Finally, we state two basic properties of characteristic maps. The first one is derived from the fact that Ψ and $A\Psi = \lambda\Psi$ join smoothly,

$$\Psi^j(1,t) = \lambda\Psi^j(2,2t) \ , \quad \Psi^j(t,1) = \lambda\Psi^j(2t,2) \ , \quad t \in [0,1] \ . \tag{2.15}$$

The second one expresses continuity between segments,

$$\Psi^j(0,t) = \Psi^{j+1}(t,0) \ , \quad t \in [1,2] \ . \tag{2.16}$$

3 Symmetry and Fourier Analysis

This section examines the special structure of the characteristic map for subdivision schemes obeying generic symmetry assumptions, namely that subdivision is independent of the particular labeling of control points used for refining the control mesh. According

to the split of $\mathbf{x}_m$ into n segments, the vectors $\mathbf{B}_m$ of control points can be divided into n equally structured blocks,

$$\mathbf{B}_m := [\mathbf{B}_m^0; \ldots; \mathbf{B}_m^{n-1}] \,, \tag{3.1}$$

and A is partitioned into $n \times n$ square blocks $A^{j,j'}, j, j' \in \mathbb{Z}_n$.

Definition 3.1 *A subdivision algorithm is called* symmetric *if it is invariant both under a shift S and a reflection R of the labeling of the vector $\mathbf{B}_m$ of control points. S and R are permutation matrices characterized by*

$$N(u, v, j+1)\mathbf{B}_m \equiv N(u, v, j) S \mathbf{B}_m \tag{3.2}$$

$$N(v, u, -j)\mathbf{B}_m \equiv N(u, v, j) R \mathbf{B}_m \,. \tag{3.3}$$

Symmetry of the subdivision algorithm means that the subdivision matrix A commutes both with R and S, i.e.

$$SA = AS \,, \quad RA = AR \,. \tag{3.4}$$

With $S^{j,j'}$ the segments of S and E the identity matrix of the same size as $S^{j,j'}$, the shift matrix S is given by

$$S^{j,j'} = \delta_{j,j'+1} E \,. \tag{3.5}$$

Comparison of SA and AS shows that the subdivision matrix of a symmetric scheme is block-cyclic, i.e.

$$A^j := A^{j,0} = A^{j+j',j'} \,, \quad j, j' \in \mathbb{Z}_n \,. \tag{3.6}$$

Thus, (2.8) becomes

$$\mathbf{B}_{m+1}^j = \sum_{j'=0}^{n-1} A^{j'} \mathbf{B}_m^{j'+j} \,, \quad j \in \mathbb{Z}_n \,. \tag{3.7}$$

With

$$\omega_n := c_n + i s_n := \exp(2\pi i/n) \tag{3.8}$$

define the *discrete Fourier transform* by

$$\hat{p}^k := \sum_{j=0}^{n-1} \omega_n^{-jk} p^j \,, \quad k \in \mathbb{Z}_n \,. \tag{3.9}$$

Here, $p = (p^0, \ldots, p^{n-1})$ is an n-vector in the generalized sense that its entries p^j can be either scalars, or vectors, or matrices. It will always become clear from the context, what is meant. Applying the discrete Fourier transform to (3.7) yields

$$\hat{\mathbf{B}}_{m+1}^k = \hat{A}^k \hat{\mathbf{B}}_m^k \,, \tag{3.10}$$

see [Lip81] for a comprehensive introduction to the Fourier analysis of cyclic systems.

Theorem 3.1 *The characteristic map for a symmetric scheme is non-injective unless the subdominant eigenvalue λ is an eigenvalue of $\hat{A}^1$ and $\hat{A}^{n-1}$.*

Proof λ is an eigenvalue of A if and only if it is an eigenvalue of $\hat{A}^k$ for some $k \in \{0, \ldots, n-1\}$. If λ is an eigenvalue of $\hat{A}^k$ then it is also an eigenvalue of $\hat{A}^{n-k}$ since A is real and $\hat{A}^{n-k} = \overline{\hat{A}}^k$. Let $\hat{A}^k\hat{\psi} = \lambda\hat{\psi}$, then

$$\psi_* := [\omega_n^0\hat{\psi}, \omega_n^k\hat{\psi}, \ldots, \omega_n^{k(n-1)}\hat{\psi}] \tag{3.11}$$

is a complex eigenvector of A. Consequently, the segments Ψ_*^j of the complex characteristic map satisfy

$$\Psi_*^j = \omega_n^{jk}\Psi_*^0 \,. \tag{3.12}$$

Now, the winding number of the closed curve

$$\alpha_*(t) : [0, \pi/2) \times \mathbb{Z}_n \ni (t, j) \mapsto \Psi_*^j(2\cos(t), 2\sin(t)) \tag{3.13}$$

is either k or $n-k$. So, if $k \notin \{1, n-1\}$ the curve α_* has self-intersections implying that Ψ_* is not injective. □

The effect of the subdominant eigenvalue λ stemming from the wrong Fourier component is depicted in Figure 2 on the right hand side. It shows the non-injective characteristic map for the Doo-Sabin algorithm for $n = 5$ with weights chosen such that λ is an eigenvalue of $\hat{A}^2$ and $\hat{A}^4$. As a consequence of Theorem 3.1, it will be assumed that λ is an eigenvalue of $\hat{A}^1$ and $\hat{A}^{n-1}$ from now on. So, (3.12) becomes

$$\Psi_*^j = \omega_n^j\Psi_*^0 \,. \tag{3.14}$$

The following lemma is the key to reducing the analysis of the characteristic map Ψ to the examination of a single segment, say Ψ^0. Ψ is called *normalized* if $\hat{\psi}$ is scaled such that $\Psi^0(2,2) = (d, 0)$ with $d > 0$. Note that normalization is always possible if Ψ is injective since then $\Psi^0(2,2) \neq \Psi^0(1,1) = \lambda\Psi^0(2,2)$.

Lemma 3.1 *If Ψ_* is a normalized characteristic map of a symmetric scheme, then*

$$\Psi_*^j(u, v) = \overline{\Psi}_*^{-j}(v, u) \,, \tag{3.15}$$

and in particular

$$\Psi_*^0(u, v) = \overline{\Psi}_*^0(v, u) \,. \tag{3.16}$$

Proof (3.2) and (3.3) yield $N(u, v, j)S^{-1}R = N(u, v, j)RS$ implying that

$$S^{-1}R = RS \tag{3.17}$$

since the functions forming N are assumed to be linearly independent. From (3.4) one concludes that $R\psi_*$ is an eigenvector of A to the eigenvalue λ, i.e. it can be written as

$$R\psi_* = a\psi_* + b\overline{\psi}_* \ , \quad a, b \in \mathbb{C} \ . \tag{3.18}$$

On using $S\psi_* = \omega_n \psi_*$, one obtains from the latter two equations

$$S^{-1}R\psi_* = a\overline{\omega}_n\psi_* + b\omega_n\overline{\psi}_* = a\omega_n\psi_* + b\omega_n\overline{\psi}_* = RS\psi_* \ . \tag{3.19}$$

Since ψ_* and $\overline{\psi}_*$ are linearly independent, this implies $a = 0$, hence $R\psi_* = b\overline{\psi_*}$. In order to determine b, consider $\Psi^0_*(2,2)$. By (3.3),

$$d = N(2,2,0)\psi_* = N(2,2,0)R\psi_* = bN(2,2,0)\overline{\psi}_* = bd \ , \tag{3.20}$$

thus $b = 1$ and $R\psi_* = \overline{\psi}_*$. Finally, we obtain

$$\Psi^j_*(u,v) = N(u,v,j)\psi_* = N(v,u,-j)\overline{\psi}_* = \overline{\Psi}^{-j}_*(v,u) \ . \tag{3.21}$$

□

4 Conditions for regularity and injectivity

In this section we derive a sequence of lemmas resulting in two sufficient conditions for the regularity and injectivity of the characteristic map that can be verified efficiently. Throughout, it will be assumed that Ψ is a normalized characteristic map of a symmetric subdivision scheme.

The first lemma states that for regular functions injectivity is equivalent to injectivity at the boundary.

Lemma 4.1 *Denote by ∂U the boundary of U and by Ψ^0_∂ the restriction of Ψ^0 to ∂U. If $\Psi^0 = [\Psi^0_1, \Psi^0_2]$ is regular, i.e.*

$$D\Psi^0 := \begin{pmatrix} \Psi^0_{1,u} & \Psi^0_{1,v} \\ \Psi^0_{2,u} & \Psi^0_{2,v} \end{pmatrix} \ , \quad J^0 := \det D\Psi^0 \neq 0 \ , \tag{4.1}$$

then Ψ^0 is injective if and only if Ψ^0_∂ is injective.

Proof Assume that Ψ^0 is regular and Ψ^0_∂ is injective. By the Inverse Function Theorem (IFT), points in the interior $\overset{\circ}{U}$ of U are mapped to points in the interior of $\Psi^0(U)$, i.e.

$$\partial\Psi^0(U) \cap \Psi^0(\overset{\circ}{U}) = \emptyset \; . \tag{4.2}$$

Define the function μ assigning the number of pre-images to the points in $\Psi^0(U)$,

$$\mu : \Psi^0(U) \ni (x,y) \mapsto \#\{(u,v) \in U : \Psi^0(u,v) = (x,y)\} \in \mathbb{N} \; . \tag{4.3}$$

Injectivity of Ψ^0_∂ and (4.2) imply $\mu(\partial\Psi^0(U)) = 1$. μ is upper semi-continuous by the IFT, hence $\mu(\Psi^0(U)) = 1$, i.e. Ψ is injective. □

The second lemma gives a sufficient condition for $\Psi^0_*(U)$ being located in a sector of angle $2\pi/n$ in the complex plane.

Lemma 4.2 *If Ψ^0 is regular and*

$$\Psi^0_{1,v}(1,t) > 0 \; , \quad \Psi^0_{2,v}(1,t) > 0 \tag{4.4}$$

for all $t \in [0,1]$, then

$$-\pi/n \leq \arg \Psi^0(u,v) \leq \pi/n \tag{4.5}$$

for all $(u,v) \in U$.

Proof By Lemma 3.1, we have

$$\Psi^0_1(u,v) = \Psi^0_1(v,u) \; , \quad \Psi^0_2(u,v) = -\Psi^0_2(v,u) \; , \tag{4.6}$$

and in particular $\Psi^0_2(t,t) = 0, t \in [1,2]$. Let $p_*(t) := p_1(t) + ip_2(t) := \Psi^0_*(1,t), t \in [0,1]$, then p_2 is monotonically increasing because $\Psi^0_{2,v} > 0$ and

$$\Psi^0_2(1,0) = p_2(0) < p_2(t) < p_2(1) = \Psi^0_2(1,1) = 0 \; , \quad t \in (0,1) \; . \tag{4.7}$$

Now, consider $\Psi^0_*(t,0), t \in [1,2]$. By (3.12), (2.16) and (3.16) we obtain for $t \in [1,2]$

$$\omega_n \Psi^0_*(t,0) = \Psi^1_*(t,0) = \Psi^0_*(0,t) = \overline{\Psi}^0_*(t,0) \; . \tag{4.8}$$

This implies either $\arg \Psi^0_*(t,0) = -\pi/n$ or $\arg \Psi^0_*(0,t) = \pi - \pi/n$. The second case contradicts (4.7), thus

$$\arg \Psi^0_*(t,0) = -\pi/n \; , \quad \arg \Psi^0_*(0,t) = \pi/n \; . \tag{4.9}$$

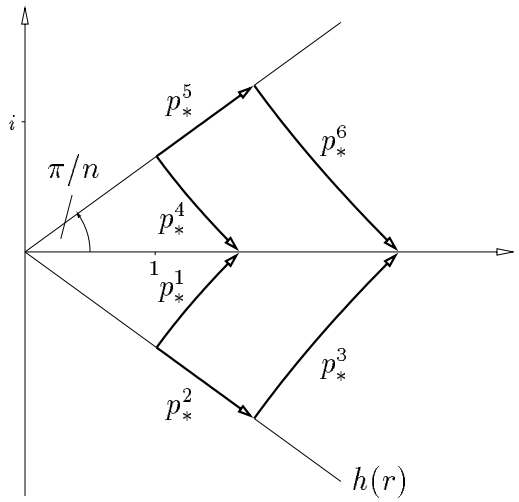

Figure 3: Curves $p_*^1, \ldots, p_*^6$.

This means that $\Psi^0(t,0)$ is a part of the straight half line $h(r) = r\exp(-i\pi/n), r > 0$. Since p_* is monotonically increasing in both real and imaginary part, it has no intersections with h except for $p_*(0)$, hence

$$-\pi/n = \arg p_*(0) < \arg p_*(t) < \arg p_*(1) = 0 \ , \quad t \in (0,1) \ . \tag{4.10}$$

Using the scaling property (2.15) and symmetry with respect to the real axis, the latter two inequations imply that (4.5) holds for all $(u,v) \in \partial U$. By the IFT, we have $\partial\Psi_*^0(U) \subset \Psi_*^0(\partial U)$, i.e. $-\pi/n \leq \arg \partial\Psi^0(U) \leq \pi/n$. Since $\Psi^0(U)$ is compact, this implies $-\pi/n \leq \arg \Psi^0(U) \leq \pi/n$ as asserted. □

The third lemma provides a condition on the partial derivatives of Ψ^0 that implies injectivity.

Lemma 4.3 *If Ψ^0 is regular and $\Psi^0_{1,v}(1,t), \Psi^0_{2,v}(1,t) > 0, t \in [0,1]$, then Ψ^0 is injective.*

Proof By Lemma 4.1 it suffices to show that the restriction Ψ^0_∂ of Ψ^0 to the boundary of U is injective. Let

$$p_*^1(t) := \Psi_*^0(1,t) \ , \quad p_*^2(t) := \Psi_*^0(1+t,0) \ , \quad p_*^3(t) := \Psi_*^0(2,2t) \tag{4.11}$$

$$p_*^4(t) := \Psi_*^0(t,1) \ , \quad p_*^5(t) := \Psi_*^0(0,1+t) \ , \quad p_*^6(t) := \Psi_*^0(2t,2) \tag{4.12}$$

for $t \in [0,1]$, see Figure 3. Then

$$p_* = p_*^1 = \overline{p}_*^4 = \lambda p_*^3 = \lambda \overline{p}_*^6 \tag{4.13}$$
$$p_*^2 = \overline{p}_*^5 \tag{4.14}$$

with $p_* = p_1 + ip_2$ defined as in the proof of Lemma 4.2. p_*^2 and p_*^5 do not intersect since

$$\arg p_*^2 = -\pi/n \ , \quad \arg p_*^5 = \pi/n \tag{4.15}$$

by (4.9). Both curves also do not have self-intersections since they are parametrized regularly and parts of straight lines. Next, we show that $\arg p_*(t)$ is monotonically increasing in t. By (4.7) and (4.9),

$$p_2(0) < 0 \ , \quad p_2(1) = 0 \ , \quad p_1(0) = p_2(0)\sin(-\pi/n) > 0 \ . \tag{4.16}$$

By assumption, p_1 and p_2 are monotone increasing, thus $p_1 > 0$ and $p_2 \leq 0$. This implies

$$\frac{d}{dt}(\arg p_*) = \frac{p_1 p_2' - p_1' p_2}{p_1^2 + p_2^2} > 0 \tag{4.17}$$

as claimed. Monotonicity of $\arg p_* = \arg p^1 = \arg p^3 = -\arg p^4 = -\arg p^6$ has the following consequences: First, it guarantees that $p_*^1, p_*^3, p_*^4, p_*^6$ do not have self-intersections. Second, it excludes intersections of p_*^1 and p_*^3 since $p_*^1 = \lambda p_*^3, \lambda \neq 1$. Analogously, p_*^4 and p_*^6 are disjoint. Third, the only intersections of p_*^1 and p_*^3 with p_*^2 are

$$\Psi_*^0(1,0) = p_*^1(0) = p_*^2(0) \tag{4.18}$$
$$\Psi_*^0(2,0) = p_*^3(0) = p_*^2(1) \ , \tag{4.19}$$

and analogously for p_*^4, p_*^5, p_*^6. Fourth, the only intersections of $p_*^1 \cup p_*^2 \cup p_*^3$ and $p_*^4 \cup p_*^5 \cup p_*^6$ are

$$\Psi_*^0(1,1) = p_*^1(1) = p_*^4(1) \tag{4.20}$$
$$\Psi_*^0(2,2) = p_*^3(1) = p_*^6(1) \ , \tag{4.21}$$

and the proof is complete. □

The following theorem establishes a sufficient condition on the partial derivatives of Ψ^0 that guarantees regularity and injectivity of the characteristic map. Its usefulness is due to the fact that it requires only estimates for the partial derivatives of the single segment Ψ^0. Since for generalized B-spline subdivision schemes the functions in questions are piecewise polynomial, the condition can be verified numerically or even analytically using B-spline representations and the convex hull property.

Theorem 4.1 *If Ψ^0 is regular and $\Psi_{1,v}^0(1,t), \Psi_{2,v}^0(1,t) > 0, t \in [0,1]$, then the characteristic map Ψ is regular and injective.*

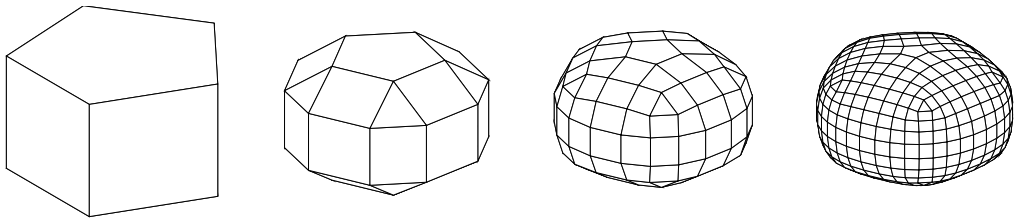

Figure 4: Mesh refinement by the Doo-Sabin algorithm.

Proof By Lemma 4.3, Ψ^0 is regular and injective. (3.14) says that Ψ^j is obtained from Ψ^0 by a $2\pi j/n$-rotation about the origin. So, each $\Psi^j, j \in \mathbb{Z}_n$ is regular and injective. Further, the segments Ψ^j do not overlap since Lemma 4.2 yields

$$(2j-1)\pi/n \leq \arg \Psi^j_* \leq (2j+1)\pi/n \ , \quad j \in \mathbb{Z}_n \ . \tag{4.22}$$

□

The assumptions of the following Corollary are stronger than those of Theorem 4.1, but can be verified with less effort since no products of partial derivatives are involved in verifying that Ψ^0 is regular.

Corollary 4.1 *If* $\Psi^0_{1,v}(u,v), \Psi^0_{2,v}(u,v) > 0$ *for all* $(u,v) \in U$, *then the characteristic map* Ψ *is regular and injective.*

Proof The symmetry relation (4.6) yields

$$D\Psi^0(u,v) = \begin{pmatrix} \Psi^0_{1,v}(v,u) & \Psi^0_{1,v}(u,v) \\ -\Psi^0_{2,v}(v,u) & \Psi^0_{2,v}(u,v) \end{pmatrix} \ , \tag{4.23}$$

so the determinant J^0 is positive if $\Psi^0_{1,v}, \Psi^0_{2,v} > 0$. □

5 The Doo-Sabin algorithm

5.1 Algorithm

The Doo-Sabin algorithm is a generalization of the subdivision scheme for biquadratic tensor product B-splines. For each n-gon of the original mesh, a new, smaller n-gon is created and connected suitably with its neighbors, see Figure 4. Figure 5 shows the

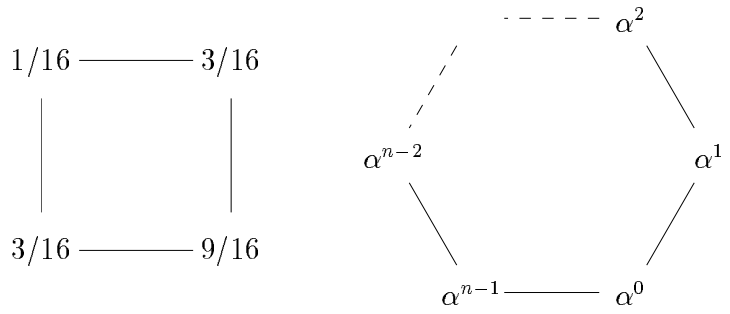

Figure 5: Masks for the Doo-Sabin algorithm.

mask for generating a new n-gon from an old one for the regular case $n = 4$ *(left)*, and the general case *(right)*. The weights suggested by Doo and Sabin in [DS78] are

$$\alpha^j = \frac{\delta_{j,0}}{4} + \frac{3 + 2\cos(2\pi j/n)}{4n} \ . \tag{5.1}$$

Below we analyze more general schemes assuming beforehand nothing but affine invariance and symmetry,

$$\sum_{j=0}^{n-1} \alpha_n^j = 1 \ , \quad \alpha^j = \alpha^{n-j} \ . \tag{5.2}$$

5.2 Characteristic map

Each of the n segments $\mathbf{x}_m^j, j \in \mathbb{Z}_n$, of the surface layers generated by the Doo-Sabin algorithm consists of 3 biquadratic B-spline patches. Accordingly, the n blocks $\mathbf{B}_m^j$ forming the vector of control points $\mathbf{B}_m$ consist of 9 elements, each. The labeling is shown in Figure 6. The 9×9-matrices $\hat{A}^k, k \in \mathbb{Z}_n$, as introduced in (3.10) have the following structure,

$$\hat{A}^k = \begin{pmatrix} \hat{\alpha}^k & 0 & 0 \\ \hat{A}_{1,0}^k & \hat{A}_{1,1}^k & 0 \\ \hat{A}_{2,0}^k & \hat{A}_{2,1}^k & 0 \end{pmatrix} \ . \tag{5.3}$$

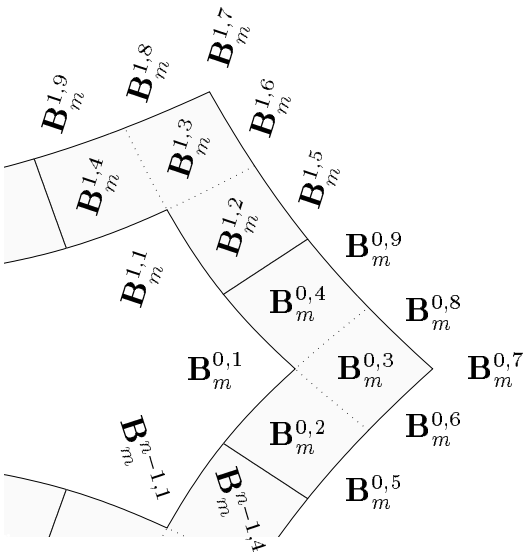

Figure 6: Labeling of control points for the Doo-Sabin algorithm

With $p := 9/16, q := 3/16, r := 1/16$, the sub-matrices are given by

$$\hat{A}_{10}^k = \begin{pmatrix} p + \overline{\omega}_n q \\ p \\ p + \omega_n q \end{pmatrix} \quad , \quad \hat{A}_{11}^k = \begin{pmatrix} q & 0 & \overline{\omega}_n r \\ q & r & q \\ \omega_n r & 0 & q \end{pmatrix}$$

$$\hat{A}_{20}^k = \begin{pmatrix} q + \overline{\omega}_n r \\ q \\ r \\ q \\ q + \omega_n r \end{pmatrix} \quad , \quad \hat{A}_{21}^k = \begin{pmatrix} p & 0 & \overline{\omega}_n q \\ p & q & r \\ q & p & q \\ r & q & p \\ \omega_n q & 0 & p \end{pmatrix} \quad . \tag{5.4}$$

The matrix $A_{1,1}^k$ has eigenvalues $1/4, 1/8, 1/16$, hence each of them is an n-fold eigenvalue of the subdivision matrix A. Further, A has a $5n$-fold eigenvalue 0 stemming from the 5×5-zero submatrix of $\hat{A}^k$. Due to their high multiplicity, these eigenvalues cannot be playing the role of the subdominant eigenvalue λ. The only eigenvalues left are the upper left entries $\hat{\alpha}^k, k \in \mathbb{Z}_n$, of $\hat{A}^k$ obtained by applying the discrete Fourier transform to the vector $(\alpha^0, \ldots, \alpha^{n-1})$ of weights for the n-gon. Since the α^j sum up to 1, we have $\lambda_0 := \hat{\alpha}_n^0 = 1$. Due to symmetry, the remaining eigenvalues are real and occur in pairs according to $\hat{\alpha}_n^k = \hat{\alpha}_n^{n-k}$. From the theory developed in the preceding sections we know that

$$\lambda := \hat{\alpha}_n^1 = \hat{\alpha}_n^{n-1} \tag{5.5}$$

must satisfy

$$1 > \lambda > \max\{1/4, |\hat{\alpha}_n^2|, \ldots, |\hat{\alpha}_n^{n-2}|\} \; . \tag{5.6}$$

The eigenvector of the matrix $\hat{A}^1$ corresponding to λ is

$$\psi_* = \begin{pmatrix} 2\lambda(16\lambda-1)(8\lambda-1)(4\lambda-1) \\ 6\lambda(16\lambda-1)(6\lambda-1+2\overline{\omega}_n\lambda) \\ 18\lambda(32\lambda^2-1+4c_n\lambda) \\ 6\lambda(16\lambda-1)(6\lambda-1+2\omega_n\lambda) \\ (16\lambda-1)\Big(12\lambda^2+18\lambda-3+\overline{\omega}_n(4\lambda^2+12\lambda-1)\Big) \\ 6\lambda\Big(32\lambda^2+64\lambda-12+c_n(20\lambda+1)-is_n(16\lambda-1)\Big) \\ 64\lambda^3+512\lambda^2-46\lambda-8+36c_n\lambda(2\lambda+1) \\ 6\lambda\Big(32\lambda^2+64\lambda-12+c_n(20\lambda+1)+is_n(16\lambda-1)\Big) \\ (16\lambda-1)\Big(12\lambda^2+18\lambda-3+\omega_n(4\lambda^2+12\lambda-1)\Big) \end{pmatrix} \; . \tag{5.7}$$

Note that the characteristic map depends only on λ and n. That is, all masks α with identical first Fourier component yield the same characteristic map.

5.3 Verification

We start with briefly discussing the case $\lambda = 1/2$ as obtained in particular for the weights in (5.1). Rearranging the entries of the eigenvector ψ_* in the more convenient matrix form for tensor product B-spline coefficients, see Figure 6, yields

$$\psi_* = 3 \begin{pmatrix} 7 & 14+7\omega_n & 21+14\omega_n \\ 14+7\overline{\omega}_n & 21+6c_n & 28+2\overline{\omega}_n+9\omega_n \\ 21+14\overline{\omega}_n & 28+2\omega_n+9\overline{\omega}_n & 35+12c_n \end{pmatrix} \; . \tag{5.8}$$

The segment Ψ_*^0 of the characteristic map consists of three bi-quadratic patches, which can be expressed in Bernstein-Bézier form with the following coefficients,

$$\frac{3}{2} \; * \; \begin{array}{ccccc} \begin{matrix} 28+10\,c_n \\ 28\,s_n \end{matrix} & \begin{matrix} 35+13\,c_n \\ 21\,s_n \end{matrix} & \begin{matrix} 42+19\,c_n \\ 14\,s_n \end{matrix} & \begin{matrix} 49+17\,c_n \\ 7\,s_n \end{matrix} & \begin{matrix} 56+20\,c_n \\ 0 \end{matrix} \\ | & | & | & | & | \\ \begin{matrix} 21+7\,c_n \\ 21\,s_n \end{matrix} & \begin{matrix} 28+14\,c_n \\ 14\,s_n \end{matrix} & \begin{matrix} 35+13\,c_n \\ 7\,s_n \end{matrix} & \begin{matrix} 42+12\,c_n \\ 0 \end{matrix} & \begin{matrix} 49+17\,c_n \\ -7\,s_n \end{matrix} \\ | & | & | & | & | \\ \begin{matrix} 14+14\,c_n \\ 14\,s_n \end{matrix} & \begin{matrix} 21+21\,c_n \\ 7\,s_n \end{matrix} & \begin{matrix} 28+10\,c_n \\ 0 \end{matrix} & \begin{matrix} 35+13\,c_n \\ -7\,s_n \end{matrix} & \begin{matrix} 42+19\,c_n \\ -14\,s_n \end{matrix} \\ & & | & & | \\ & & \begin{matrix} 21+7\,c_n \\ -7\,s_n \end{matrix} & \begin{matrix} 28+14\,c_n \\ -14\,s_n \end{matrix} & \begin{matrix} 35+21\,c_n \\ -21\,s_n \end{matrix} \\ & & | & & | \\ & & \begin{matrix} 14+14\,c_n \\ -14\,s_n \end{matrix} & \begin{matrix} 21+21\,c_n \\ -21\,s_n \end{matrix} & \begin{matrix} 28+28\,c_n \\ -28\,s_n \end{matrix} \end{array} \tag{5.9}$$

Computing the partial derivative $\Psi^0_{*,v} = \Psi^0_{1,v} + i\Psi^0_{2,v}$ with respect to v yields three quadratic-linear patches with coefficients

$$\frac{3}{2} \quad * \quad \begin{array}{ccccccc} 14+14\,c_n & & 14+14\,c_n & & 14+12\,c_n & & 14+10\,c_n & & 14+6\,c_n \\ 14\,s_n & & 14\,s_n & & 14\,s_n & & 14\,s_n & & 14\,s_n \\ & & & & | & & & & | \\ 14+14\,c_n & & 14+14\,c_n & & 14+6\,c_n & & 14-2\,c_n & & 14-4\,c_n \\ 14\,s_n & & 14\,s_n & & 14\,s_n & & 14\,s_n & & 14\,s_n \\ & & & & | & & & & | \\ & & & & 14-14\,c_n & & 14-14\,c_n & & 14-14\,c_n \\ & & & & 14\,s_n & & 14\,s_n & & 14\,s_n \end{array} \tag{5.10}$$

Both the real and the imaginary part of the coefficients are positive. So, by the convex hull property and Corollary 4.1 the algorithm is verified to generate smooth limit surfaces.

The situation for general λ is more subtle, in particular as $\lambda \to 1$. First, Corollary 4.1 turns out to be insufficient. Second, there exists a limit value $\lambda_{\max}(n) < 1$ depending on n such that even the assumptions of Theorem 4.1 are not fulfilled for $1 > \lambda > \lambda_{\max}$. It will be shown in the next subsection that this is due to an actual loss of smoothness as λ passes the bound. All formulas required here were derived using a computer algebra system. They are partially rather lengthy and will not be stated explicitly unless necessary. Rather, we depict the crucial results graphically.

In order to apply Theorem 4.1, we have to compute J^0, i.e. the determinant of the Jacobian of Ψ^0. J^0 is a continuous, piecewise bi-cubic function over U which can be expressed in Bernstein-Bézier form with 3×16 coefficients $J^0_\mu, \mu = 1, \ldots, 48$ depending on n and λ. Explicit calculation shows that all coefficients J^0_μ are of the form

$$J^0_\mu(c_n, \lambda) = s_n(16\lambda - 1)(P_\mu(\lambda) + c_n Q_\mu(\lambda)) \tag{5.11}$$

with P_μ, Q_μ polynomials of degree ≤ 6 in λ. We give the coefficient corresponding to $J^0(1,1)$ the index $\mu = 1$, i.e.

$$J^0(1,1) = J^0_1 = s_n(16\lambda - 1)(P_1 + c_n Q_1)\ . \tag{5.12}$$

The polynomials P_1 and Q_1 are

$$P_1(\lambda) := 96\lambda^3(-128\lambda^3 + 128\lambda^2 - 7\lambda - 2) \tag{5.13}$$

$$Q_1(\lambda) := 864\lambda^4\ . \tag{5.14}$$

In order to apply analytic tools, it is convenient to consider c_n as a free variable varying in the interval $c_n \in [-1/2, 1]$, which covers all possible values obtained for $n \geq 3$. For fixed $\lambda \in (1/4, 1)$ there is at most one value $\tilde{c}_n$ where J^0_μ changes sign,

$$\tilde{c}_n = R_\mu(\lambda) := -P_\mu(\lambda)/Q_\mu(\lambda)\ . \tag{5.15}$$

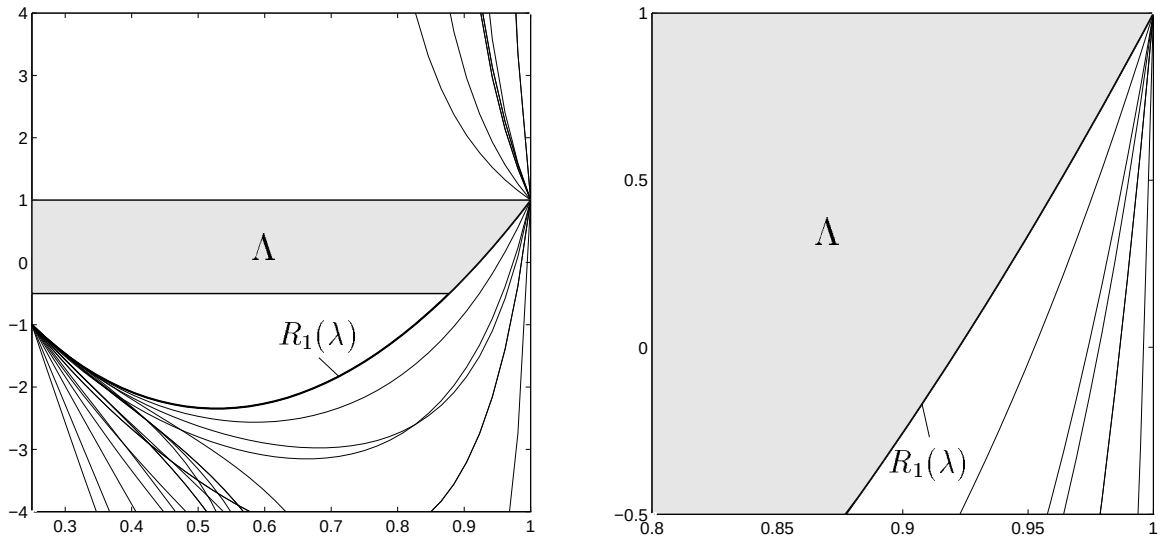

Figure 7: Feasible set Λ and functions $R_\mu(\lambda)$.

Figure 7 shows a plot of all these functions as well as a magnification of the significant region. From the analysis of the case $\lambda = 1/2$ we know that $J^0_\mu(c_n, 1/2) > 0$ for all μ. Thus, J^0 is positive as long as (λ, c_n) lies in the shaded region, which is bounded by $R_1(\lambda)$. More precisely, the feasible set for (λ, c_n) providing positivity of J^0 is

$$\Lambda := \{(\lambda, c_n) \in (1/4, 1) \times [-1/2, 1] : J^0_1(c_n, \lambda) > 0\} \; . \tag{5.16}$$

For the verification of the assumptions of Theorem 4.1 it remains to show that $\Psi^0_{1,v}(1,t)$, $\Psi^0_{2,v}(1,t) > 0$ for $t \in [0,1]$ and $(c_n, \lambda) \in \Lambda$. Note that both functions are linear in t. So, it suffices to check positivity for $t \in \{0,1\}$, which follows immediately from

$$\Psi^0_{1,v}(1,0) = 2\lambda(16\lambda - 1)(4\lambda - 1)(4\lambda + 1)(1 - c_n) \tag{5.17}$$

$$\Psi^0_{2,v}(1,0) = 2\lambda(16\lambda - 1)(4\lambda - 1)(4\lambda + 1)s_n \tag{5.18}$$

$$\Psi^0_{2,v}(1,1) = 12 s_n \lambda^2 (16\lambda - 1) \tag{5.19}$$

$$\Psi^0_{1,v}(1,1) = J^0_1 \,/\, 2\Psi^0_{2,v}(1,1) \; . \tag{5.20}$$

Finally, we summarize the results derived in this section.

Theorem 5.1 *Let $\alpha^0_n, \ldots, \alpha^{n-1}_n$ be symmetric weights for the Doo-Sabin algorithm. If $\lambda := \hat{\alpha}^1_n = \hat{\alpha}^{n-1}_n$ satisfies*

$$1 > \lambda > \max\{1/4, |\hat{\alpha}^2_n|, \ldots, |\hat{\alpha}^{n-2}_n|\} \tag{5.21}$$

$$128\lambda^2(1 - \lambda) - 7\lambda - 2 + 9\lambda\cos(2\pi/n) > 0 \; , \tag{5.22}$$

then the limit surface $\mathbf{y}$ is a regular C^1-manifold for almost every choice of initial data $\mathbf{B}_0$.

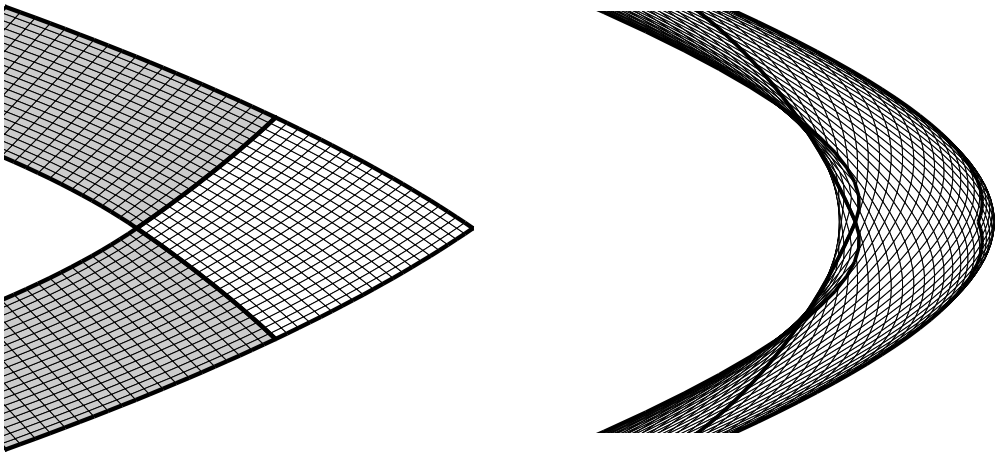

Figure 8: Characteristic map for $n = 3$ and $\lambda = 0.5$ *(left)* and $\lambda = 0.95$ *(right)*.

5.4 Failure beyond the bound

In contrast to the lower bound $\lambda > 1/4$, which appears naturally, the existence of an *upper* bound for λ may come as a surprise. It is not an artifact of the particular type of sufficient conditions in Theorem 4.1, but a sharp bound beyond which the Doo-Sabin algorithm provably fails. If $J_1^0 < 0$ then

$$\Psi_{2,v}^0(1,1) = 12 s_n \lambda^2 (16\lambda - 1) > 0 \tag{5.23}$$

$$\Psi_{1,v}^0(1,1) = J_1^0 \,/\, 2\Psi_{2,v}^0(1,1) < 0 \,. \tag{5.24}$$

Consider the curve $[g_1(t), g_2(t)] := \Psi^0(t,t)$. Symmetry with respect to the x-axis implies $g_2(t) \equiv 0$. For the first component we obtain

$$g_1'(1) = 2\Psi_{1,v}(1,1) < 0 \;, \quad g_1(1) = \Psi_1^0(1,1) < \lambda \Psi_1^0(2,2) = g_1(2) \;, \tag{5.25}$$

hence for each sufficiently small $\varepsilon > 0$ there exists an $\varepsilon' > \varepsilon$ such that $g_1(1+\varepsilon) = g_1(1+\varepsilon')$. This implies the non-injectivity of the characteristic map Ψ,

$$\Psi^0(1+\varepsilon, 1+\varepsilon) = \Psi^0(1+\varepsilon', 1+\varepsilon') \;, \quad \varepsilon \neq \varepsilon' \,. \tag{5.26}$$

Moreover, for ε sufficiently small, $J^0(1+\varepsilon, 1+\varepsilon) < 0$ by continuity. So, $\Psi^0(1+\varepsilon, 1+\varepsilon)$ is an interior point of $\Psi(U, \mathbb{Z}_n)$ by the IFT, and the assumptions of Theorem 2.2 are fulfilled proving sharpness of the bound. Figure 8 shows a magnification of the characteristic map for $n = 3$ in the vicinity of $\Psi^0(1,1)$ for $\lambda = 1/2$ *(left)* and $\lambda = 0.95$ *(right)*. The latter case corresponds to weights $\alpha^0 = 0.9667$, $\alpha^1 = \alpha^2 = 0.01667$. Six layers of a subdivision

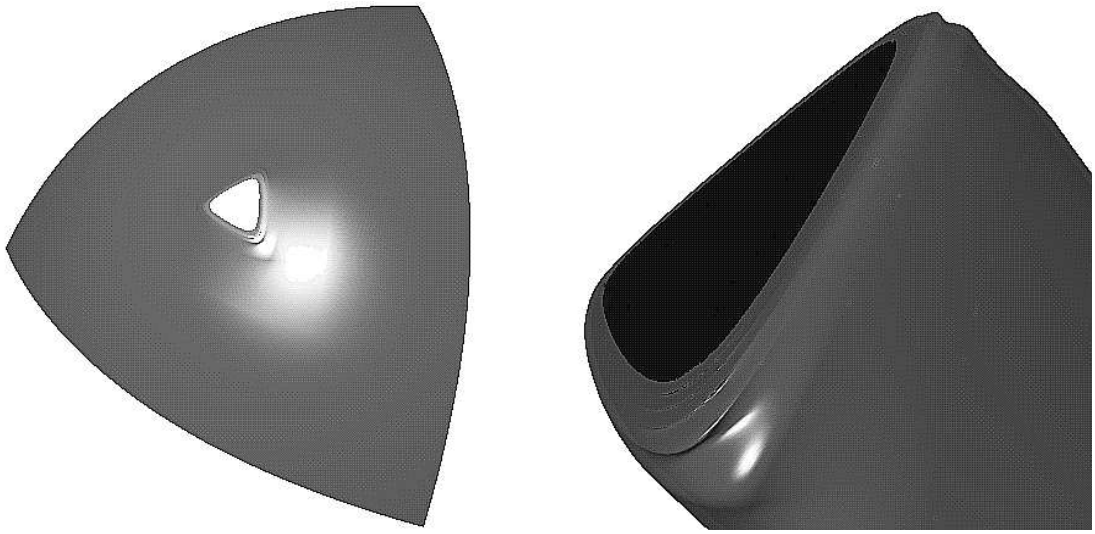

Figure 9: Non-smooth surface generated by the Doo-Sabin algorithm with $\lambda = 0.95$.

surface generated by these weights are shown in Figure 9. The magnification on the right hand side is non-proportional, i.e. the 'height' of the surface has been expanded in order to depict its wavy shape. We conclude the discussion of the Doo-Sabin algorithm with a brief description of the qualitative and quantitative behavior of $\lambda_{\max}(n)$. As $n \to \infty$, $\lambda_{\max}(n)$ is increasing monotonically towards 1. The asymptotic behavior for large n is

$$\lambda_{\max}(n) = 1 - \frac{\pi^2}{7n^2} + O(n^{-4}) \; . \tag{5.27}$$

The lowest bound occurs for $n = 3$, namely

$$\lambda_{\max}(3) = \frac{\sqrt{187}}{24} \cos\left(\frac{1}{3} \arctan\left(\frac{27\sqrt{5563}}{1576}\right)\right) + \frac{1}{3} \approx 0.8773 \; . \tag{5.28}$$

Table 1 lists the values of $\lambda_{\max}$ for $n = 3, \ldots, 12$.

6 The Catmull-Clark algorithm

6.1 Algorithm

The Catmull-Clark algorithm is a generalization of the subdivision scheme for bicubic tensor product B-splines. Each n-gon of the original mesh is subdivided into n quadrilaterals thus generating a purely quadrilateral mesh after the first step. There are three masks for subdividing such a mesh, namely one for computing a new centroid, one for

n	$\lambda_{\max}(n)$	n	$\lambda_{\max}(n)$
3	0.8772872432	8	0.9786066941
4	0.9223409885	9	0.9829902941
5	0.9478340134	10	0.9861607079
6	0.9628618416	11	0.9885250887
7	0.9723152935	12	0.9903339733

Table 1: Values of the bound $\lambda_{\max}(n)$ for $n = 3, \ldots, 12$.

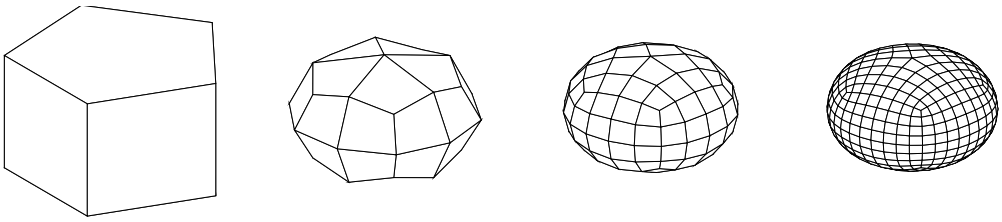

Figure 10: Mesh refinement by the Catmull-Clark algorithm.

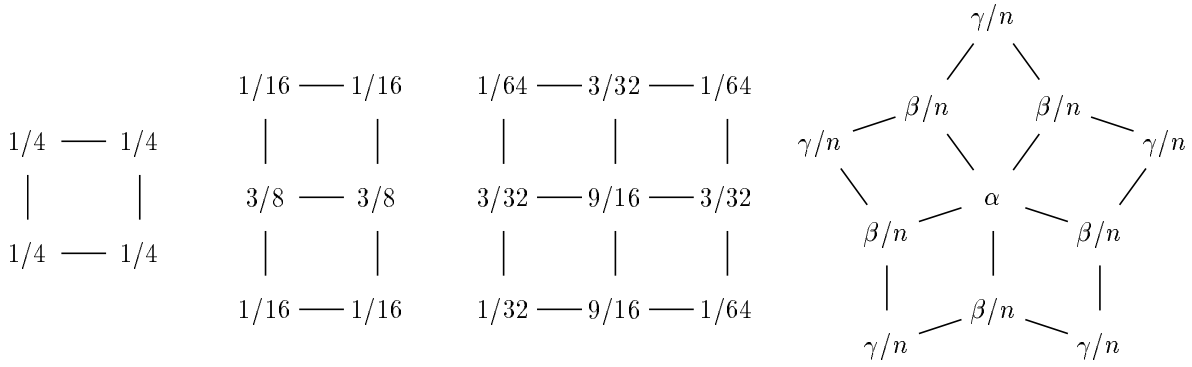

Figure 11: Masks for the Catmull-Clark algorithm.

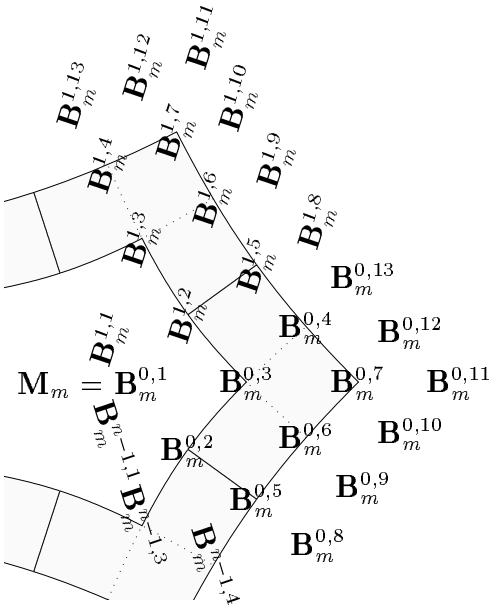

Figure 12: Labeling of control points for the Catmull-Clark algorithm.

a new edge point, and one for the new location of a former vertex, see Figure 11. So, the variables at our disposal are the weights

$$\alpha\,,\ \beta\,,\ \gamma\,,\quad \alpha+\beta+\gamma=1\,. \tag{6.1}$$

In [CC78], Catmull and Clark suggest

$$\alpha = 1-\frac{7}{4n}\,,\ \beta=\frac{3}{2n}\,,\ \gamma=\frac{1}{4n}\,. \tag{6.2}$$

6.2 Characteristic map

Each of the n segments $\mathbf{x}_m^j, j\in\mathbb{Z}_n$, of the surface layers generated by the Catmull-Clark algorithm consists of 3 bicubic B-spline patches. Accordingly, the n blocks $\mathbf{B}_m^j$ forming the vector of control points $\mathbf{B}_m$ consist of 13 elements, each. The labeling used here is shown in Figure 12. Note that the centroid

$$\mathbf{M}_m := \mathbf{B}_m^0 = \cdots = \mathbf{B}_m^{n-1} \tag{6.3}$$

is replaced by n identical copies in order to achieve the desired periodic structure. For all masks involving $\mathbf{M}_m$ we substitute

$$\mathbf{M}_m = \frac{1}{n}\sum_{j=0}^{n-1}\mathbf{B}_m^j\,. \tag{6.4}$$

The 13×13-matrices $\hat{A}^k, k \in \mathbb{Z}_n$, turn out to have the following structure,

$$\hat{A}^k = \begin{pmatrix} \hat{A}^k_{0,0} & 0 & 0 \\ \hat{A}^k_{1,0} & \hat{A}^k_{1,1} & 0 \\ \hat{A}^k_{2,0} & \hat{A}^k_{2,1} & 0 \end{pmatrix} . \tag{6.5}$$

With

$$p_1 := 1/64\,,\ p_2 := 3/32\,,\ p_3 := 9/16\,,\ q_1 := 1/16\,,\ q_2 := 3/8\,,\ r := 1/4\ , \tag{6.6}$$

the sub-matrices are given by

$$\hat{A}^k_{0,0} = \begin{pmatrix} \alpha\delta_{k,0} & \beta\delta_{k,0} & \gamma\delta_{k,0} \\ q_2\delta_{k,0} & 2q_1c_n + q_2 & q_1(1+\overline{\omega}_n) \\ r\delta_{k,0} & r(1+\omega_n) & r \end{pmatrix} \tag{6.7}$$

$$\begin{pmatrix} \hat{A}^k_{1,0} & \hat{A}^k_{1,1} \\ \hat{A}^k_{2,0} & \hat{A}^k_{2,1} \end{pmatrix} = \left(\begin{array}{ccc|ccc|c} q_2\delta_{k,0} & q_1 + q_2\omega_n & q_1 & q_1 & q_1\omega_n & 0 & 0 \\ p_2\delta_{k,0} & 2p_1c_n + p_3 & p_2(1+\overline{\omega}_n) & p_1\overline{\omega}_n & p_2 & p_1 & 0 \\ q_1\delta_{k,0} & q_1\omega_n + q_2 & q_2 & 0 & q_1 & q_1 & 0 \\ p_1\delta_{k,0} & p_2(1+\omega_n) & p_3 & p_2 & p_1(1+\omega_n) & p_2 & p_1 \\ \hline 0 & q_2 & q_1(1+\overline{\omega}_n) & q_1\overline{\omega}_n & q_2 & q_1 & 0 \\ 0 & r & r & 0 & r & r & 0 \\ 0 & q_1 & q_2 & q_1 & q_1 & q_2 & q_1 \\ 0 & 0 & r & r & 0 & r & r \\ 0 & q_1\omega_n & q_2 & q_2 & q_1\omega_n & q_1 & q_1 \\ 0 & r\omega_n & r & r & r\omega_n & 0 & 0 \end{array}\right)$$

The eigenvalues $1/8, 1/16, 1/32, 1/64$ of the sub-matrix $\hat{A}^k_{1,1}$ are n-fold eigenvalues of A. Other non-zero eigenvalues come only from $\hat{A}^k_{0,0}$. For $k = 0$ we obtain the obligatory eigenvalue $\lambda_0 = 1$ and, letting $\gamma := 1 - \alpha - \beta$,

$$\lambda^0_{1,2} = \left(4\alpha - 1 \pm \sqrt{(4\alpha-1)^2 + 8\beta - 4}\right)/8\ , \tag{6.8}$$

which might be either both real or complex conjugate. For $k \neq 0$, the non-zero eigenvalues of $\hat{A}^k_{0,0}$ are

$$\lambda^k_1 = \left(c_{n,k} + 5 + \sqrt{(c_{n,k}+9)(c_{n,k}+1)}\right)/16 \tag{6.9}$$

$$\lambda^k_2 = \left(c_{n,k} + 5 - \sqrt{(c_{n,k}+9)(c_{n,k}+1)}\right)/16\ , \tag{6.10}$$

where $c_{n,k} := \cos(2\pi k/n)$. Let

$$\lambda := \lambda^1_1 = \lambda^{n-1}_1 = \left(c_n + 5 + \sqrt{(c_n+9)(c_n+1)}\right)/16\ , \tag{6.11}$$

then straightforward calculus shows that for all n

$$1 > \lambda > 1/4 > \lambda_2^k > 1/8 \ , \quad k = 1, \ldots, n-1 \tag{6.12}$$

$$\lambda > \lambda_1^k > 1/4 \ , \qquad k = 2, \ldots, n-2 \ . \tag{6.13}$$

Consequently, λ is subdominant if α, β, γ are chosen such that

$$\lambda > \max\{|\lambda_1^0|, |\lambda_2^0|\} \ . \tag{6.14}$$

In particular, this inequality holds for the original weights of Catmull-Clark (6.2), as can be verified by inspection. A characterization of feasible positive weights can be found in [BS88][2]. For computing the characteristic map, the eigenvector $\hat{\psi}$ of $\hat{A}^1$ is partitioned into three blocks, $\hat{\psi} = [\hat{\psi}_0, \hat{\psi}_1, \hat{\psi}_2]$, according to the special structure of $\hat{A}^1$. Then $\hat{A}^1\hat{\psi} = \lambda\hat{\psi}$ is equivalent to

$$\begin{aligned} (\hat{A}^1_{0,0} - \lambda)\hat{\psi}_0 &= 0 \\ (\hat{A}^1_{1,1} - \lambda)\hat{\psi}_1 &= -\hat{A}^1_{1,0}\hat{\psi}_0 \\ \hat{\psi}_2 &= (\hat{A}^1_{2,0}\hat{\psi}_0 + \hat{A}^1_{2,1}\hat{\psi}_1)/\lambda \ . \end{aligned} \tag{6.15}$$

Now, $\hat{\psi}$ can be computed conveniently starting from

$$\hat{\psi}_0 := [1 + \overline{\omega}_n, 16\lambda - 2c_n - 6]^T \ , \tag{6.16}$$

which solves the first eigenvector equation. Note that the characteristic map depends only on n, and not on the particular choice of weights α, β, γ provided that (6.11) holds.

6.3 Verification

Corollary 4.1 is sufficient for verifying the algorithm. One proceeds as follows:

1. For given $n \geq 3$, compute the subdominant eigenvalue λ according to (6.11) and the corresponding eigenvector $\hat{\psi}$ according to (6.15).

2. Express the three patches of the segment Ψ^0 of the characteristic map in Bernstein-Bézier form.

3. Compute the forward differences $\Delta_\mu, \mu = 1, \ldots, 36$, of Bézier coefficients corresponding to the partial derivative with respect to v.

4. If all $\Delta_\mu, \mu = 1, \ldots, 36$ are positive in both components, then by the convex hull property of the Bernstein-Bézier form the assumptions of Corollary 4.1 are fulfilled and the characteristic map is regular and injective.

[2]The result in the reference is incorrect for $n = 3$ and certain α, β yielding complex eigenvalues $\lambda_{1,2}^0$.

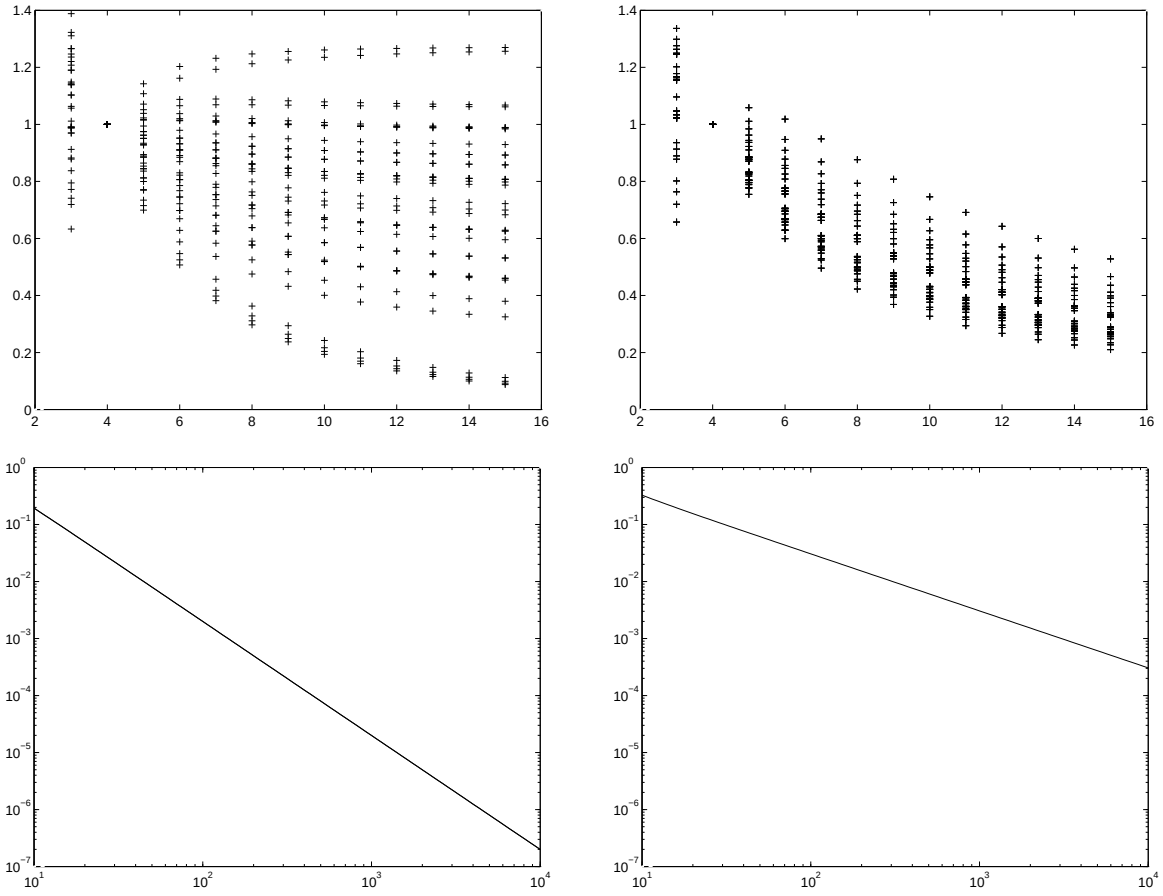

Figure 13: Bézier coefficients of the partial derivatives Δ_μ.

This procedure can be run on a computer algebra system, but the resulting expressions are rather lengthy, and discussing them is not very instructive. A numerical treatment is more convenient and yields equally reliable results since only a finite number of quantities has to be checked for sign. The findings are summarized on Figure 13. The left and right hand side correspond to the two components of Δ_μ. The top row shows the values of all Δ_μ for $n = 3, \ldots, 20$. The bottom row shows the minimum of the Δ_μ on a doubly-logarithmic scale for $n = 10, \ldots, 10,000$, which should cover most cases of practical relevance. The positivity of all differences is evident. By Corollary 4.1, this proves smooth convergence of the Catmull-Clark algorithm provided that the inequality (6.14) holds.

References

[BS86] A. A. Ball and D. J. T. Storry, *A matrix approach to the analysis of recursively generated b-spline surfaces*, Computer Aided Design **18** (1986), 437–442.

[BS88] A. A. Ball and D. J. T. Storry, *Conditions for tangent plane continuity over recursively generated b-spline surfaces*, ACM Trans. on Graphics **7** (1988), 83–102.

[CC78] E. Catmull and J. Clark, *Recursively generated B-spline surfaces on arbitrary topological meshes*, Computer Aided Design **10** (1978), 350–355.

[DS78] D. Doo and M. A. Sabin, *Behaviour of recursive subdivision surfaces near extraordinary points*, Computer Aided Design **10** (1978), 356–360.

[Lip81] J. D. Lipson, *Elements of algebra and algebraic computing*, Addison-Wesley, 1981.

[PR97] H. Prautzsch and U. Reif, *Necessary conditions for subdivision surfaces*, Tech. report, Sonderforschungsbereich 404, Universität Stuttgart, 1997, Report 97/04.

[Rei95a] U. Reif, *A unified approach to sudivision algorithms near extraordinary vertices*, Computer Aided Geometric Design **12** (1995), 153–174.

[Rei95b] Ulrich Reif, *Some new results on subdivision algorithms for meshes of arbitrary topology*, Wavelets and Multilevel Approximation (C. K. Chui and L. L. Schumaker, eds.), Series in Approximations and Decompositions, vol. 2, World Scientific, 1995, pp. 367–374.